USGS
science for a changing world

Radiometric Ages of Volcanic Rocks on the Fort Rock Dome and in the Aquarius Mountains, Yavapai and Mohave Counties, Arizona

Open-File Report 2019–1038

U.S. Department of the Interior
U.S. Geological Survey

COVER. Satellite image of study area south of Interstate 40 near the border between Mohave county and Yavapai county, Arizona.

Radiometric Ages of Volcanic Rocks on the Fort Rock Dome and in the Aquarius Mountains, Yavapai and Mohave Counties, Arizona

By Gary S. Fuis, Andrew Calvert, and Katie Sullivan

Open-File Report 2019–1038

U.S. Department of the Interior
U.S. Geological Survey

U.S. Department of the Interior
DAVID BERNHARDT, Secretary

U.S. Geological Survey
James F. Reilly II, Director

U.S. Geological Survey, Reston, Virginia: 2019

Suggested citation:
Fuis, G.S., Calvert, A., and Sullivan, K., 2019, Radiometric ages of volcanic rocks on the Fort Rock dome and in the Aquarius Mountains, Yavapai and Mohave counties, Arizona: U.S. Geological Survey Open-File Report 2019–1038, 18 p., https://doi.org/10.3133/ofr20191038.

ISSN 2331-1258 (online)

Contents

Figures

Tables

Conversion Factors

International System of Units to U.S. customary units

Multiply	By	To obtain
Length		
meter (m)	3.281	foot (ft)
kilometer (km)	0.6214	mile (mi)
Area		
square kilometer (km^2)	247.1	acre
square kilometer (km^2)	0.3861	square mile (mi^2)
Mass		
gram (g)	0.03527	ounce, avoirdupois (oz)

Temperature in degrees Celsius (°C) may be converted to degrees Fahrenheit (°F) as

$$°F = (1.8 \times °C) + 32.$$

Temperature in degrees Fahrenheit (°F) may be converted to degrees Celsius (°C) as

$$°C = (°F - 32) / 1.8.$$

Abbreviations

HPTA	hornblende-pyroxene trachyandesite
Ma	mega annum
m.y.	duration of millions of years
OTB	olivine trachybasalt
RWB	welded rhyodacite breccia
RDD	rhyodacite dike
TRIGA	U.S. Geological Survey training, research, isotopes, and general atomics
USGS	U.S. Geological Survey
XRF	X-ray fluorescence

Radiometric Ages of Volcanic Rocks on the Fort Rock Dome and in the Aquarius Mountains, Yavapai and Mohave Counties, Arizona

By Gary S. Fuis, Andrew Calvert, and Katie Sullivan

Abstract

The Fort Rock dome, in Yavapai County, Ariz., is a roughly circular geologic structure in plan view, 2.5 km in diameter, that is similar in many ways to an impact crater; however, it is a structural dome caused by a potassic mafic intrusion at depth, and the craterlike depression in its center is erosional in origin. The Aquarius Mountains, west of the Fort Rock dome, in Mohave County, contain a felsic volcanic center that erupted tuffs, non-welded ash-flow tuffs, and lahars following dome emplacement.

This report discusses the radiometric ages of samples of rock units from both the Fort Rock dome and the Aquarius Mountains eruptive center. The ages for all samples span a short interval of time from 22.3 to 21.7 m.y. (earliest Miocene). The individual sample ages are consistent with the stratigraphic order of the rock units in the area, and the short age span is consistent with the absence of any significant unconformities in the section.

Introduction

The Fort Rock dome, in Yavapai County, Ariz., and the adjacent Aquarius Mountains to the west, in Mohave County, were most recently mapped in the late 1960's and early 1970's by Fuis (1973, 1996) (figs. 1, 2). The motivation for mapping the dome, which appears as a distinctive circular crater on aerial photographs, was to determine whether or not it originated as a meteorite impact crater. The motivation for mapping the eruptive center west of the dome was to establish the sequence of volcanic events as they related to dome emplacement. The Aquarius Mountains eruptive center appeared to be a major center for ash-flow tuffs and other felsic volcanic units in a region extending from the dome to the west edge of the Colorado Plateau Transition Zone, approximately 16 km west of the dome. Other mapping in the region now includes an east-west strip map north of Fort Rock dome extending approximately along the corridor of current Interstate 40 (Goff and others, 1983) and mapping of the Mohon Mountains and Hope Mountain volcanic fields south and southeast of the dome (Simmons, 1990; Simmons and Ward, 1992). Ages acquired from the Fort Rock dome and Aquarius Mountains eruptive center will establish a chronology of volcanic events in these locations and will lead to their placement in the context of more recent geologic mapping in the region. Samples from the Fort Rock dome and Aquarius Mountains eruptive center are earliest Miocene (22.3 to 21.7 Ma) and samples from the Mohon Mountains and Hope Mountain volcanic fields range in age from early to late Miocene (22–5 Ma; Simmons and Ward, 1992). The Peach Spring Tuff (18.78 Ma; Ferguson and others, 2013) separates rocks of the Aquarius Mountains and Mohon Mountains volcanic fields where they overlap (Simmons and Ward, 1992).

Geologic Setting

Rocks exposed in the vicinity of the Fort Rock dome range in age from Precambrian to Quaternary. Precambrian igneous and metamorphic rocks and Tertiary volcanic rocks are the primary units that are exposed in this area (fig. 2). Volcanic rocks crop out over an area about 2,600 km^2 in extent largely north, west, and south of the dome, in both Yavapai and Mohave counties, Ariz., but other volcanic fields are present eastward to the San Francisco peaks, near Flagstaff, Ariz. (Goff and others, 1983). Numerous volcanic centers are scattered throughout the vicinity of the Fort Rock dome, which is one relatively small center. The slightly younger Aquarius Mountains rhyodacite eruptive center, located 8 km southwest of the dome's center, is larger, with dimensions from rim to rim ranging from 3-5 km (Fuis, 1996) (figs. 1, 2). The chief structure in the vicinity of the dome is an east-west-striking fault that curves southeastward near the dome's SW flank (Fuis, 1996) (fig. 2). This fault postdates rocks of the Aquarius Mountains eruptive center. Faults of other orientations are present, including northerly striking basin-and-range faults near the Cottonwood Cliffs, west of Fort Rock dome (Goff and others, 1983) (figs. 1, 2). Most Phanerozoic rocks are relatively flat lying. The Fort Rock dome is an anomalous area where Tertiary rocks are folded and faulted (Fuis, 1996).

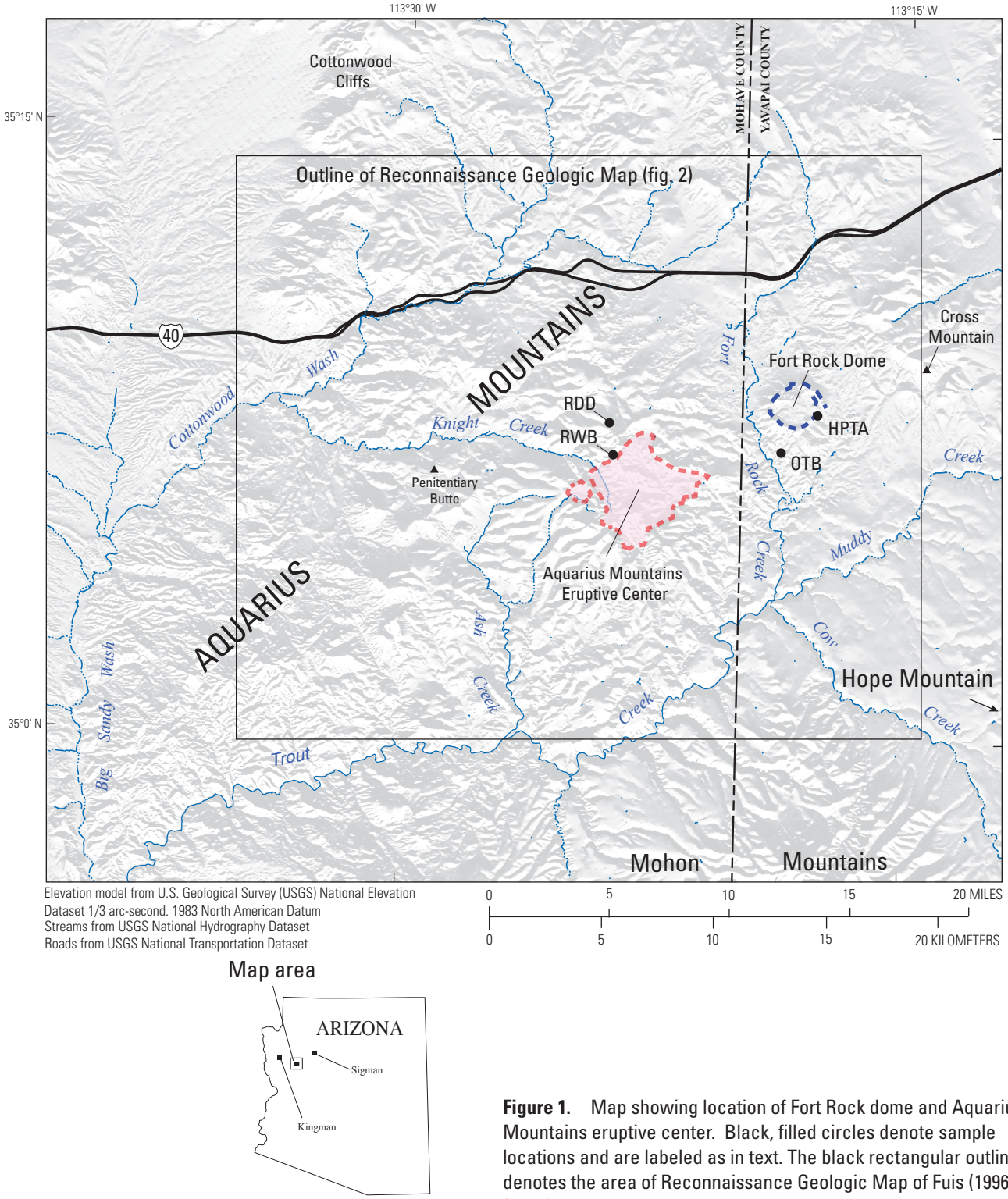

Figure 1. Map showing location of Fort Rock dome and Aquarius Mountains eruptive center. Black, filled circles denote sample locations and are labeled as in text. The black rectangular outline denotes the area of Reconnaissance Geologic Map of Fuis (1996) (fig. 2).

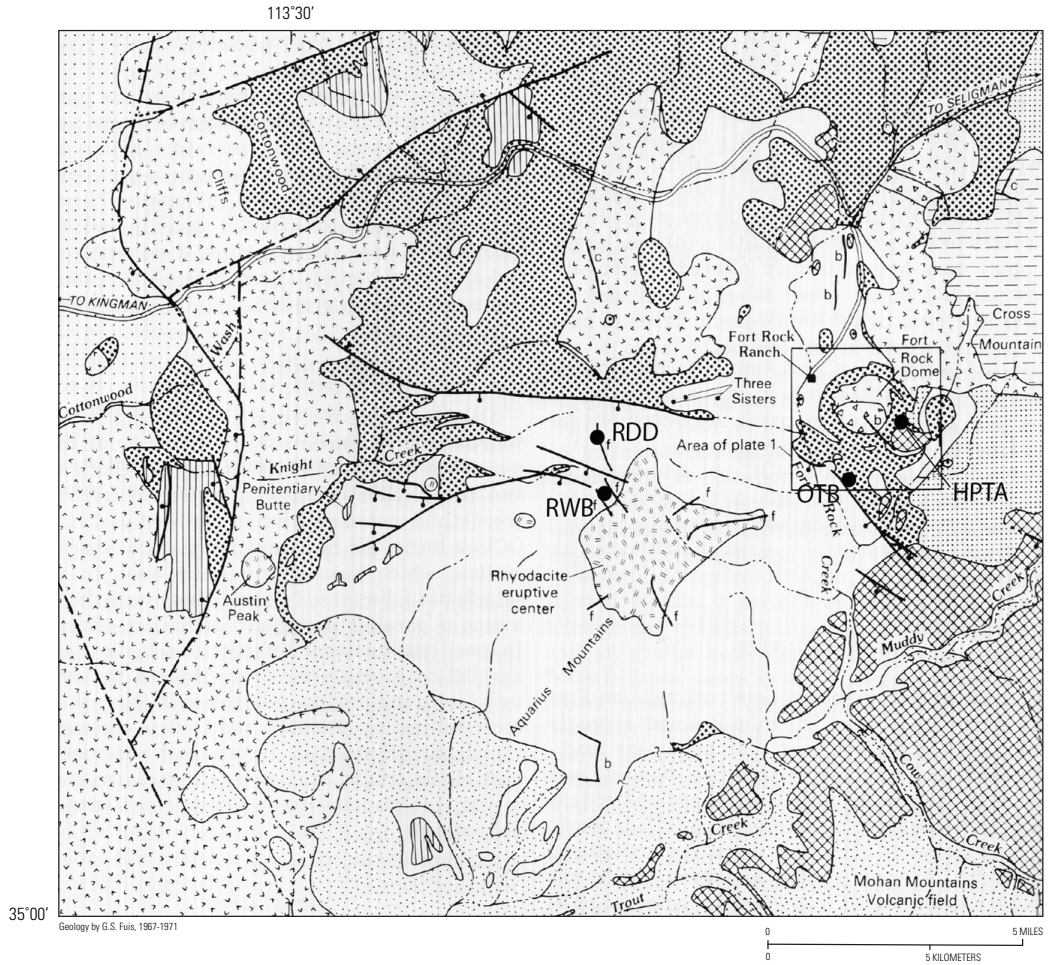

EXPLANATION

Quaternary

Surficial deposits—Wide-spaced dots indicate alluvium; close-spaced dots, terrace deposits

Unconformity

Tertiary

Peach Springs Tuff of Young (1966)

Uncomformity (?)

Fort Rock Creek Rhyodacite—Pattern indicates intrusive rock

Crater Pasture Formation

Andesite and basalt

Rhyodacite and dacite

Undivided volcanic and sedimentary rocks

Unconformity

Paleozoic

Redwall Limestone, unnamed Devonian carbonate rock, Muav Limestone, Bright Angel Shale, and Tapeats Sandstone

Unconformity

Precambrian

Layered metamorphic rocks, cataclasites, granite, and pegmatite—Triangles indicate Precambrian shear zone

—?— **Contact**—Queried where uncertain

Fault—Dashed where uncertain; bar and ball on downthrown side

c **Dike**—b, basalt or andesite
f, Fort Rock Creek Rhyodacite
c, Crater Pasture Formation

Figure 2. The reconnaissance geologic map of Fuis (1996; his fig. 3). Sample locations (from our fig. 1) are plotted on this map. The rectangle labeled "Area of Plate 1" is the area of the detailed geologic map in Fuis (1996).

Rock Units

Precambrian rocks on or near Fort Rock dome include layered metamorphic rocks of epidote-amphibolite facies that are intruded (or apparently intruded) by two separate groups of granitic rocks; one group crushed and foliated along with the host rocks and the other group crushed but not foliated. The entire assemblage resembles older Precambrian rocks in the Grand Canyon. On the dome, the Precambrian rocks are fractured and veined in an east-west-trending shear zone that crosses the south half of the dome. Most fracturing and veining in this zone is Precambrian in age (Fuis, 1996).

Tertiary volcanic rocks overlie a lower to middle Tertiary erosion surface that covered most of northwest Arizona (Young and McKee, 1978). In the vicinity of the Fort Rock dome, these rocks comprise two formations, the Crater Pasture Formation and Fort Rock Creek Rhyodacite; the Crater Pasture Formation is ultramafic to intermediate in composition and older, and the Fort Rock Creek Rhyodacite is felsic and younger (Fuis, 1996). Volcanic rocks in the region younger than these two formations include the Peach Spring Tuff, of middle Miocene age (Young and Brennan, 1974; Ferguson and others, 2013), which overlies the Fort Rock Creek Rhyodacite 16 km west of the dome, and the Mohon Mountains volcanic field, south of Trout Creek, which overlies the Peach Spring Tuff (Simmons, 1990; Simmons and Ward, 1992).

The Crater Pasture Formation includes ultramafic to intermediate lava flows, agglomerates, tuffs, and associated intrusive and sedimentary rocks on the Fort Rock dome in an area of about 300 km^2 largely west, north, and south of the dome. Eleven subunits are recognized in the vicinity of the dome. Most of the rocks in these subunits originated from vents on or near the periphery of the Fort Rock dome and are traceable for distances of 2 km or less. The youngest unit in the formation is an olivinesanidine-trachybasalt flow, referred to as the "flow of Fault Canyon" (Fuis, 1996). This flow was erupted from a vent on the southwest flank of the dome and is interpreted to have come from a magma body beneath the dome that caused the doming.

The Fort Rock Creek Rhyodacite includes ash-flow and other massive tuffs, volcanic breccias, lava flows, and associated intrusive and sedimentary rocks in the Aquarius Mountains and vicinity. Four subunits are recognized; two are major rock units in the area and are designated members. The older member is the Old Stage Road Member, a unit consisting chiefly of non-welded ash-flow tuff. The younger member is the Three Sisters Butte Member, a unit of interbedded volcanic breccia and massive tuff. Most of the Fort Rock Creek Rhyodacite was erupted from the large center in the Aquarius Mountains, the center of which is located approximately 8 km southwest of the Fort Rock dome's center.

Structure

Precambrian structures on the dome include folds of different amplitudes in the layered metamorphic rocks and an east-west trending shear zone in the south half of the dome that brings together different rock assemblages and rocks of slightly different metamorphic grade. This shear zone appears to be associated with a major aeromagnetic discontinuity in Precambrian rocks in northwest Arizona (Sauck and Sumner, 1971), and we infer it to be a zone of weakness along which the body of magma was intruded that ultimately created the Fort Rock dome.

Tertiary structures on the dome include relatively minor faults that predate the uplift of the dome and the dome itself, with its associated folds and faults. The dome is a structural dome with its central part now deeply eroded (Fuis, 1996). Its edge is, in most places, a sharp circular monocline, approximately 2.5 km in diameter. Structural relief on the dome is 400 m. Dips on the steeply dipping limb of the monocline, where dips can be measured accurately, range from about 40° to nearly vertical and average about 66°. Units of the Crater Pasture Formation older than the Fault Canyon flow reflect these strong dips, whereas the Fault Canyon flow and units of the Fort Rock Creek Rhyodacite dip much more gently on the circular monocline. Most observable faults on the dome are confined to the vicinity of the monocline, perhaps partly as a result of poor exposure and lack of structural control in the deeply eroded central part of the dome. These faults have chiefly radial and tangential strikes and steep dips, where attitudes can be determined. Normal dip-slip movement appears to have been dominant, although radial faults may have had a strike-slip component of movement. Block rotations are observed along relatively long faults. Ages of faults, where they can be determined, range from the beginning of uplift, which was signaled by deposition of a sedimentary breccia on the flanks of the dome ("sedimentary breccia of One O'Clock Wash" and "sedimentary breccia of Noon Gorge" of Fuis, 1996), to after the emplacement of the ash-flow tuff (Old Stage Road Member) of the Fort Rock Creek Rhyodacite. The major offsets, however, appear to have occurred during the deposition of sedimentary breccia. In addition to mapped faults on the rim of the crater, abundant small faults with displacements of centimeters to several meters and lenses of largely unmineralized breccia were formed during doming. These are best seen in the Precambrian rocks within the crater.

The history of doming at the Fort Rock dome includes an initial stage of accelerating uplift followed by slower uplift or collapse upon formation of a vent for the magma. Domal uplift ceased upon crystallization of the magma (Fuis, 1996).

Sample Description

Two samples from the Crater Pasture Formation and two samples of the overlying Fort Rock Creek Rhyodacite have been radiometrically dated (table 1; figs. 1, 2). The two samples from the Crater Pasture Formation include a stratigraphically lower hornblende-pyroxene trachyandesite ("flow of Lion Ridge"; Fuis, 1996), that was deformed on the dome, and the olivine-sanidine trachybasalt ("flow of Fault Canyon"; Fuis, 1996) that is interpreted to have been erupted on the southwest flank of the dome from the magma body that caused the doming (Fuis, 1996). The two samples from the Fort Rock

Creek Rhyodacite are a welded rhyodacite breccia that appears to be laterally equivalent to the ash-flow tuff of the Old State Road Member and a rhyodacite dike that intrudes both members of the Fort Rock Creek Rhyodacite.

Modal and chemical/normative compositions of the two samples of the Crater Pasture Formation are given in Fuis (1996; his tables 2 and 3, respectively). The hornblende-pyroxene trachyandesite is similar to sample 154f in both of those tables; the olivine-sanidine trachybasalt is similar to samples 406a and 406b in those tables. All four of the samples that were radiometrically dated in this report were examined in thin section, new modal estimates were performed, and X-ray fluorescence (XRF) chemical analyses were obtained (tables 2 and 3).

Table 1. Tabulated sample locations

[Elevation of each sample is given in both feet (ft) and meters (m)]

Sample	Latitude N.	Longitude W.	Elevation (ft)	Elevation (m)
HPTA	35º 08’ 00.8”	113º17’ 52.0”	5,114	1,559
OTB	35º 07’ 10.7”	113º18’ 48.1”	4,942	1,506
RWB	35º 07’ 03.5”	113º23’ 31.3”	5,759	1,755
RDD	35º 06’ 50.2”	113º23’ 38.82”	5,784	1,763
[1]F78-85	35º 12’	113º25’		
[1]BA78-73	35º 14’	113º20’		
[1]F78-88	35º 11’	113º18’		

[1]Prior radiometrically dated samples in region of the Fort Rock dome and Aquarius Mountains, as discussed in the text

Table 2. Sample mineral compositions in weight percent

Sample	Hornblende-pyroxene trachyandesite (HPTA) from east side of Fort Rock dome	
Mineral	%	Description
plagiocase	50.3	laths in groundmass
k-spar	20	macro-phenocrysts with irregular outlines
quartz	0	
augite	10.9	1.8% grains in cores of pseudomorphs after hornblende macro-phenocrysts; 9.1% micro-phenocrysts and groundmass grains
pigeonite	0	
hornblende*	12.2	*pseudomorphs after macro-phenocrysts
biotite	0	
olivine	0	
alteration products		(12.2%—see pseudomorphs above)
opaque minerals	5.5	equant granules
apatite	1.4	
calcite	0.5	
Total	100.8	

Table 2. Sample mineral compositions in weight percent—Continued

Sample	Olivine-sanidine trachybasalt (OTB) from SW. flank of Fort Rock dome	
Mineral	%	Description
plagiocase	0	
k-spar	75	subhedral laths in groundmass
quartz	0	
augite	11	7% macro-phenocrysts, 4% micro-phenocrysts
pigeonite	2.2	mostly laths in groundmass; some overgrowths on augite
hornblende	0	
biotite*	1	*pseudomorphs after biotite micro-phenocrysts
olivine*	5	*pseudomorphs after olivine macro- and micro-phenocrysts
alteration products		(6%—see pseudomorphs above)
opaque minerals	0	
glass or aphanitic/low-birefringent material	0	
apatite	3.4	micro-prisms
calcite	1.6	amorphous, microcrystalline
Total	99.2	

Sample	Welded rhyodacite breccia (RWB) from west side of Aquarius Mountains eruptive center	
Mineral	%	Description
plagiocase	8.5	twinned, zoned; 1% micro-phenocrysts
k-spar	4	cleavage; even extinction; 1% micro-phenocrysts
quartz	1.5	macro- and micro-phenocrysts
pyroxene	0	
hornblende	2	
biotite	2	
olivine	0	
alteration products		
opaque minerals	0	
glass or aphanitic/low-birefringent material	82	clear glass to low-birefringent matrix; includes a few fragments of occluded/low-birefringent glass; most macro- and micro-phenocrysts of feldspar and quartz are broken, but a few are embayed
Total	100	

Table 2. Sample mineral compositions in weight percent—Continued

Sample	Rhyodacite dike (RDD) from NW. of Aquarius Mountains eruptive center	
Mineral	%	Description
plagiocase	7.5	5% macro-phenocrysts and ~ 2.5% micro-phenocrysts; twinned, zoned
k-spar	2.5	~2.5% micro-phenocrysts; square outlines, zoned
quartz	0	nothing clearly quartz as macro- or micro-phenocrysts
pyroxene	0	
hornblende	3	macro- and micro-phenocrysts; some alteration on edges
biotite	4	macro- and micro-phenocrysts; alteration on edges
olivine	0	
alteration products		altered edges on hornblende and biotite; amounts included in hornblende and biotite % estimates
opaque minerals	3	
glass or aphanitic/low-birefringent material	80	low-birefringent matrix
Total	100	

Table 3. Chemical and normative compositions in weight percent (wt %)

Oxide	HPTA	154f	Diff	OTB	406a	Diff	RWB	RDD
SiO_2	54.17	54.80	−0.63	53.15	54.10	–0.95	66.77	64.32
TiO_2	1.15	1.11	0.04	0.95	0.95	0.00	0.41	0.68
Al_2O_3	15.80	16.00	−0.20	12.76	13.30	–0.54	15.38	15.84
Fe_2O_3			0.00			0.00		
FeO	7.40	8.01	−0.61	5.61	7.00	–1.39	2.54	4.00
MnO	0.13	0.13	0.00	0.07	0.03	0.04	0.05	0.05
MgO	4.66	3.70	0.96	5.63	6.20	–0.57	1.10	1.61
CaO	7.52	7.10	0.42	8.76	6.50	2.26	2.55	3.20
Na_2O	3.83	3.80	0.03	2.13	2.10	0.03	3.92	4.32
K_2O	2.58	2.90	−0.32	5.65	5.50	0.15	4.05	3.95
P_2O_5	0.72	0.59	0.13	0.69	0.74	–0.05	0.17	0.42
CO_2	0.00	0.05	−0.05		0.05	–0.05		
Total	97.94	98.19	–0.25	95.41	96.47	–1.06	96.93	98.40

Table 3. Chemical and normative compositions in weight percent (wt %)—Continued

Minerals	Normative HPTA (wt %)	OTB (wt %)	RWB (wt %)	RDD (wt %)
Quartz	0.00	0.00	20.65	13.56
Plagioclase	51.75	26.45	46.06	49.53
Orthoclase	15.60	34.98	24.70	23.70
Nepheline	0.00	0.78	0.00	0.00
Leucite	0.00	0.00	0.00	0.00
Kalsilite	0.00	0.00	0.00	0.00
Corundum	0.00	0.00	0.35	0.00
Diopside	12.11	25.95	0.00	0.83
Hypersthene	12.68	0.00	7.03	10.10
Wollastonite	0.00	0.00	0.00	0.00
Olivine	3.94	8.25	0.00	0.00
Larnite	0.00	0.00	0.00	0.00
Acmite	0.00	0.00	0.00	0.00
K_2SiO_3	0.00	0.00	0.00	0.00
Na_2SiO_3	0.00	0.00	0.00	0.00
Rutile	0.00	0.00	0.00	0.00
Ilmenite	2.22	1.88	0.80	1.31
Magnetite	0.00	0.00	0.00	0.00
Hematite	0.00	0.00	0.00	0.00
Apatite	1.69	1.69	0.42	1.00
Zircon	0.00	0.00	0.00	0.00
Perovskite	0.00	0.00	0.00	0.00
Chromite	0.00	0.00	0.00	0.00
Sphene	0.00	0.00	0.00	0.00
Pyrite	0.00	0.00	0.00	0.00
Halite	0.00	0.00	0.00	0.00
Fluorite	0.00	0.00	0.00	0.00
Anhydrite	0.00	0.00	0.00	0.00
Na_2SO_4	0.00	0.00	0.00	0.00
Calcite	0.00	0.00	0.00	0.00
Na_2CO_3	0.00	0.00	0.00	0.00
Total	99.99	99.98	100.01	100.03

Hornblende-Pyroxene Trachyandesite (HPTA)

Hornblende-pyroxene trachyandesite (HPTA; "flow of Lion Ridge"; Fuis, 1996) is the youngest of seven lava flows that are deformed in the circular monocline of the Fort Rock dome. It crops out around parts of the northeastern and eastern rims of the erosional crater on the dome. It contains as phenocrysts 12 percent pseudomorphs after hornblende and 2 percent augite (in the cores of pseudomorphs after hornblende). In the groundmass, it contains 50 percent plagioclase laths, 20 percent large poikilitic, irregular grains of K-spar, 9 percent augite, 5.5 percent opaque minerals (as equant granules), and 1.4 percent apatite (table 2). XRF chemical analysis of this sample gives 54.2 percent SiO_2 and 2.6 percent K_2O (table 3).

Olivine Trachybasalt (OTB)

Olivine trachybasalt (OTB; "flow of Fault Canyon;" Fuis, 1996) is the largely undeformed flow and intrusive unit that crops out along the southwestern flank of the Fort Rock dome. This unit is interpreted to have been erupted from a magma chamber beneath the dome that caused the doming. It contains as phenocrysts 7 percent augite and 5 percent olivine (or alteration products). In the groundmass, it contains 75 percent subhedral laths of K-spar, 4 percent augite, 3.4 percent apatite, 2.2 percent pigeonite (some as overgrowths on augite), 1.6 percent calcite, and 1 percent pseudomorphs after biotite and olivine (table 2). XRF chemical analysis of this sample gives 53.2 percent SiO_2 and 5.6 percent K_2O (table 3).

Welded Rhyodacite Breccia (RWB)

Welded rhyodacite breccia (RWB) occurs along the western rim of the erosional lowland that overlies the Aquarius Mountains rhyodacite eruptive center (Fuis, 1996; fig. 2). It represents welding of agglomerate clasts stratigraphically below it by rhyodacite lava flows stratigraphically above it, and is interpreted to be, along with the agglomerate below it, the lateral equivalent of the Old Stage Road Member (non-welded ash-flow tuff) of the Fort Rock Creek Rhyodacite. It contains as phenocrysts 8.5 percent twinned, zoned, broken and embayed plagioclase (including 1 percent microphenocrysts), 4 percent K-spar (including 1 percent microphenocrysts), 1.5 percent quartz (including both phenocrysts and microphenocrysts), 2 percent biotite, and 2 percent hornblende. In the groundmass, it contains 82 percent glass and low-birefringent material (table 2). XRF chemical analysis of this sample gives 66.8 percent SiO_2 and 4.0 percent K_2O (table 3).

Rhyodacite Dike (RDD)

The rhyodacite dike (RDD) extends northwestward from the western rim of the Aquarius Mountains rhyodacite eruptive center and intrudes units up through the exposed Three Sisters Butte Member of the Fort Rock Creek Rhyodacite (Fuis, 1996; fig. 2). Monoliths of this dike rock are seen along the top of the ridge intruded by this unit. It contains as phenocrysts 7.5 percent twinned and zoned plagioclase (including 2.5 percent

microphenocrysts), 2.5 percent square, zoned plagioclase (chiefly as microphenocrysts), 4 percent biotite (as both phenocrysts and microphenocrysts), 3 percent hornblende (as both phenocrysts and microphenocrysts), and 3 percent opaque minerals. In the groundmass, it contains 80 percent low-birefringent material (table 2). XRF chemical analysis of this sample gives 64.3 percent SiO_2 and 4.0 percent K_2O (table 3).

Radiometric Dating Method

$^{40}Ar/^{39}Ar$ geochronology was performed on single crystals of sanidine and plagioclase and on volcanic groundmass concentrates. Minerals and groundmass separates were segregated from bulk sample by crushing, sieving, heavy liquid, and magnetic techniques. Minerals were picked under a binocular microscope. For irradiation, 16–34 milligram (mg) separates were packaged in aluminum foil and placed in a cylindrical quartz vial together with fluence monitors of known age (Taylor Creek sanidine) and K-glass and fluorite to measure interfering isotopes from K and Ca. Samples and monitor materials were irradiated for ten hours in the central thimble of the U.S. Geological Survey training, research, isotopes, and general atomics (TRIGA) reactor in Denver, Colorado (Dalrymple and others, 1981). The reactor vessel was rotated continuously during irradiation to avoid lateral neutron flux gradients. Reactor constants determined for these irradiations were indistinguishable from recent irradiations, and a weighted mean of constants obtained over the past five years yields $^{40}Ar/^{39}Ar_K = 0.0098\pm0.0002$, $^{39}Ar/^{37}Ar_{Ca} = 0.000662\pm0.00001$, and $^{36}Ar/^{37}Ar_{Ca} = 0.000275\pm0.000003$. Sanidine from the Taylor Creek Rhyolite (TCR-2; Dalrymple and Duffield, 1988) was used as a fluence monitor with an age of 28.345 ± 0.012 m.y. (Fleck and Calvert, 2016). TCR-2 is a secondary standard calibrated against the primary intralaboratory standard, GA1550 biotite, that has an age of 98.79 ± 0.54 m.y. (Renne and others, 1998). Fluence monitors and unknowns were analyzed using a continuous CO_2 laser system and mass spectrometer described by Dalrymple (1989). Unknowns were heated in a resistance furnace with temperatures monitored by an infrared pyrometer. Gas was purified continuously during extraction using two SAES ST-175 getters, one operated hot (4 amps) and the other at room temperature.

Mass spectrometer discrimination is monitored by analyzing splits of atmospheric Ar from a reservoir attached to the extraction line, and for these samples $D_{1amu} = 1.010651 \pm 0.000161$. Typical system blanks including mass spectrometer backgrounds were $1.5x10^{-18}$ mol of mass/charge number (m/z) 36, $9x10^{-17}$ mol of m/z 37, $3x10^{-18}$ mol of m/z 39, and $1.5x10^{-16}$ mol of m/z 40, where m/z is mass/charge ratio. Error bars reported below are 1σ.

Dating Results

A groundmass concentrate from sample HPTA yielded a plateau age of 22.3 ± 0.03 m.y. using 59 percent of the ^{39}Ar released. Rejected steps suggest minor ^{39}Ar recoil. The isochron age is concordant at 22.4 ± 0.08 m.y. (tables 4, 5; fig. 3). We prefer the plateau date of 22.3 ± 0.03 m.y. as the eruption age of the HPTA flow.

Groundmass from sample OTB yielded a serially decreasing age spectrum with ages ranging from 23 to 21.3 Ma. We interpret the discordance to be due to ^{39}Ar recoil and calculate a recoil model age (Fleck and others, 2014) of 22.1 ± 0.2 m.y. using 100 percent of the ^{39}Ar released (tables 4, 5;

Table 4. $^{40}Ar/^{39}Ar$ ages from the Fort Rock dome and the Aquarius Mountains.

[Preferred ages are listed in bold; MSWD, Mean sum weighted deviates; Ma, mega-annum; $^{40}Ar/^{36}Ar_i$, ratio at intercept]

Sample	Material	Age (Ma)	$^{40}Ar/^{39}Ar$ Weighted mean plateau age $\%^{39}Ar$ [steps, °C]	MSWD	Age (Ma)	$^{40}Ar/^{39}Ar$ isotope correlation (isochron) age $\%^{39}Ar$ [steps, °C]	MSWD	$^{40}Ar/^{36}Ar_i$	$^{40}Ar/^{39}Ar$ total gas Age (Ma)	Comments
RDD	Plagioclase	**21.7 ± 0.03**	50 [1,050−1,200]	0.53	21.7 ± 0.1	50 [1,050−1,200]	0.73	309.7 ± 202.1	21.7 ± 0.03	Plateau Age
RWB	Sanidine	**21.7 ± 0.03**	57 [800−1,100]	3.00	21.7 ± 0.03	57 [800−1,100]	2.85	280.7 ± 110.5	21.8 ± 0.02	Plateau Age
OTB	Ground-mass	**22.1 ± 0.2R**	100 [550−1,250]	114.33	22.2 ± 0.09	100 [550−1,250]	158.37	143.4 ± 141.2	22.1 ± 0.02	Recoil Age
HPTA	Ground-mass	**22.3 ± 0.03**	59 [750−1,050]	0.92	22.4 ± 0.08	59 [750−1,050]	0.79	278.6 ± 32.8	22.3 ± 0.02	Plateau Age

Samples irradiated at USGS TRIGA reactor using 9.797 Ma Bodie Hills sanidine as a neutron flux monitor; R, recoil model age.

Table 5. Tabulated radiometric data of HPTA groundmass

[Reduced with Taylor Creek Sanidine at 28.345 ± 0.012 Ma; Ma, mega-annum; ^{40}Ar*, radiogenic argon; ^{40}Ar—^{36}Ar, measured isotopes in volts (1.48E-13 moles/volt), corrected for blank, background, discrimination, and decay; temperature is in degrees Celsius]

Temp (°C)	Age(Ma)	%^{40}Ar*	K/Ca	K/Cl	moles ^{40}Ar*	∑^{39}Ar	^{40}Ar	^{39}Ar	^{38}Ar	^{37}Ar	^{36}Ar
550	22.1±0.3	55.64	0.64	514	2.81E-14	0.02	0.341383 ±0.000805	0.036113 ±0.000074	0.000874 ±0.000015	0.029547 ±0.001471	0.000520 ±0.000009
600	22.6±0.1	78.91	0.79	1,573	6.39E-14	0.05	0.547573 ±0.000477	0.080036 ±0.000100	0.001348 ±0.000012	0.052891 ±0.001617	0.000405 ±0.000009
650	22.9±0.1	88.85	0.86	2,609	1.43E-13	0.13	1.088467 ±0.000389	0.176996 ±0.000124	0.002704 ±0.000015	0.108087 ±0.001729	0.000440 ±0.000008
700	22.6±0.0	92.07	0.98	6,980	1.87E-13	0.24	1.375883 ±0.000413	0.234677 ±0.000162	0.003310 ±0.000054	0.125472 ±0.000713	0.000403 ±0.000008
750	22.3±0.0	93.42	1.05	5,419	2.14E-13	0.36	1.553273 ±0.000463	0.272441 ±0.000146	0.003875 ±0.000093	0.135505 ±0.000793	0.000382 ±0.000008
800	22.2±0.0	94.29	1.08	2,789	2.00E-13	0.47	1.433215 ±0.000471	0.254515 ±0.000164	0.003802 ±0.000115	0.123647 ±0.000711	0.000310 ±0.000007
850	22.3±0.0	94.58	1	2,464	1.84E-13	0.58	1.316602 ±0.000375	0.234219 ±0.000146	0.003544 ±0.000023	0.123171 ±0.001733	0.000275 ±0.000007
900	22.3±0.0	93.47	0.86	1,340	1.58E-13	0.67	1.143939 ±0.000363	0.201155 ±0.000136	0.003346 ±0.000048	0.122077 ±0.000850	0.000286 ±0.000007
975	22.2±0.0	92.42	0.75	834	1.47E-13	0.75	1.073825 ±0.000400	0.186938 ±0.000138	0.003481 ±0.000034	0.129953 ±0.000961	0.000311 ±0.000007
1,050	22.2±0.1	90.21	0.64	478	1.34E-13	0.83	1.006127 ±0.000349	0.171440 ±0.000116	0.003864 ±0.000040	0.140314 ±0.000909	0.000371 ±0.000007
1,150	21.7±0.0	87.83	0.3	54	2.35E-13	0.97	1.810691 ±0.000509	0.306988 ±0.000166	0.028588 ±0.000126	0.527678 ±0.005002	0.000890 ±0.000009
1,250	21.3±0.1	69.12	0.04	47	5.37E-14	1	0.525162 ±0.000208	0.072143 ±0.000103	0.007612 ±0.000020	0.933607 ±0.003612	0.000805 ±0.000008

Table 6. Tabulated radiometric data of OTB groundmass

[Reduced with Taylor Creek Sanidine at 28.345 ± 0.012 Ma; Ma, mega-annum; ^{40}Ar*, radiogenic argon; ^{40}Ar—^{36}Ar, measured isotopes in volts (1.48E-13 moles/volt), corrected for blank, background, discrimination, and decay; temperature is in degrees Celsius]

Temp (°C)	Age(Ma)	%^{40}Ar*	K/Ca	K/Cl	moles ^{40}Ar*	∑^{39}Ar	^{40}Ar	^{39}Ar	^{38}Ar	^{37}Ar	^{36}Ar
550	23.3±0.2	88.43	0.86	679	3.73E-14	0.01	0.285628 ±0.000308	0.045315 ±0.000067	0.000905 ±0.000027	0.027774 ±0.000358	0.000119 ±0.000007
600	23.1±0.1	92.79	0.75	905	1.17E-13	0.03	0.854290 ±0.000515	0.143515 ±0.000159	0.002614 ±0.000120	0.100910 ±0.001114	0.000236 ±0.000008
650	22.9±0.0	95.12	1.04	2,172	2.65E-13	0.08	1.886327 ±0.000486	0.327842 ±0.000284	0.005032 ±0.000171	0.165417 ±0.002173	0.000357 ±0.000009
700	22.5±0.0	97.54	2.3	3,169	3.54E-13	0.15	2.457457 ±0.000753	0.445814 ±0.000303	0.006523 ±0.000096	0.101529 ±0.001541	0.000232 ±0.000008
750	22.3±0.0	99.23	4.05	12,467	4.69E-13	0.24	3.197321 ±0.001014	0.594155 ±0.000310	0.008058 ±0.000157	0.076911 ±0.001467	0.000104 ±0.000006
800	22.1±0.0	99.51	4.28	7,433	6.99E-13	0.38	4.755471 ±0.001428	0.892466 ±0.000365	0.012303 ±0.000124	0.109288 ±0.002088	0.000109 ±0.000007
850	22.0±0.0	99.46	4.94	7,031	7.41E-13	0.53	5.040759 ±0.001712	0.950524 ±0.000455	0.013136 ±0.000094	0.100856 ±0.000298	0.000120 ±0.000007
900	22.0±0.0	99.27	5.42	3,096	6.76E-13	0.67	4.609833 ±0.001387	0.868940 ±0.000297	0.012688 ±0.000096	0.084086 ±0.000777	0.000137 ±0.000007
950	22.0±0.0	99.23	5.44	2,007	5.12E-13	0.77	3.494824 ±0.001416	0.658804 ±0.000329	0.010116 ±0.000042	0.063520 ±0.000833	0.000109 ±0.000007

Table 6. Tabulated radiometric data of OTB groundmass—Continued

[Reduced with Taylor Creek Sanidine at 28.345 ± 0.012 Ma; Ma, mega-annum; ^{40}Ar*, radiogenic argon; ^{40}Ar—^{36}Ar, measured isotopes in volts (1.48E-13 moles/volt), corrected for blank, background, discrimination, and decay; temperature is in degrees Celsius]

Temp (°C)	Age(Ma)	%^{40}Ar*	K/Ca	K/Cl	moles ^{40}Ar*	∑^{39}Ar	^{40}Ar	^{39}Ar	^{38}Ar	^{37}Ar	^{36}Ar
1,025	21.9±0.0	98.78	4.22	776	4.46E-13	0.86	3.055405 ±0.002911	0.575268 ±0.000417	0.010795 ±0.000078	0.071474 ±0.001249	0.000145 ±0.000008
1,100	21.8±0.0	97.76	2.32	337	3.72E-13	0.93	2.572058 ±0.000856	0.480867 ±0.000234	0.012501 ±0.000086	0.108555 ±0.001079	0.000224 ±0.000007
1,175	21.6±0.0	94.9	0.38	39	1.96E-13	0.98	1.398446 ±0.000577	0.257323 ±0.000135	0.031632 ±0.000169	0.352398 ±0.001911	0.000338 ±0.000008
1,250	21.7±0.1	96.1	0.09	101	1.22E-13	1	0.860127 ±0.000285	0.159858 ±0.000106	0.008885 ±0.000051	0.942331 ±0.001948	0.000372 ±0.000008

Table 7. Tabulated radiometric data of RWB sanidine

[Reduced with Taylor Creek Sanidine at 28.345 ± 0.012 Ma; Ma, mega-annum; ^{40}Ar*, radiogenic argon; ^{40}Ar—^{36}Ar, measured isotopes in volts (1.48E-13 moles/volt), corrected for blank, background, discrimination, and decay; temperature is in degrees Celsius]

Temp (°C)	Age (Ma)	%^{40}Ar*	K/Ca	K/Cl	moles ^{40}Ar*	∑^{39}Ar	^{40}Ar	^{39}Ar	^{38}Ar	^{37}Ar	^{36}Ar
600	20.4±0.2	77.6	3.53	221	3.58E-14	0	0.312407 ±0.000877	0.049036 ±0.000065	0.001644 ±0.000109	0.007283 ±0.001005	0.000238 ±0.000009
700	21.6±0.1	96.35	7.55	1649	1.44E-13	0.02	1.012749 ±0.000384	0.186424 ±0.000228	0.002968 ±0.000130	0.012963 ±0.001165	0.000128 ±0.000007
750	21.8±0.0	98.59	12.14	20,735	1.86E-13	0.04	1.273364 ±0.000435	0.237443 ±0.000186	0.003193 ±0.000018	0.010265 ±0.000380	0.000064 ±0.000007
800	21.7±0.0	98.8	20.23	-2,354,795	3.13E-13	0.07	2.145867 ±0.000536	0.403755 ±0.000222	0.005341 ±0.000065	0.010473 ±0.000516	0.000090 ±0.000007
850	21.7±0.0	99.19	19.67	37,465	4.64E-13	0.12	3.168540 ±0.000929	0.597659 ±0.000221	0.007968 ±0.000089	0.015943 ±0.000506	0.000091 ±0.000007
900	21.7±0.0	99.3	27.44	64,050	6.60E-13	0.19	4.502349 ±0.001360	0.851067 ±0.000358	0.011303 ±0.000074	0.016276 ±0.000443	0.000111 ±0.000007
950	21.7±0.0	99.47	26.91	35,648	7.08E-13	0.27	4.815804 ±0.001508	0.910034 ±0.000312	0.012129 ±0.000089	0.017743 ±0.000676	0.000092 ±0.000008
1,000	21.7±0.0	99.33	30.9	27,990	9.49E-13	0.37	6.469797 ±0.002314	1.222572 ±0.000390	0.016341 ±0.000056	0.020758 ±0.000329	0.000152 ±0.000008
1,050	21.7±0.0	99.64	30.44	10,569	1.12E-12	0.49	7.639330 ±0.002298	1.446113 ±0.000501	0.019679 ±0.000120	0.024930 ±0.000644	0.000100 ±0.000008
1,100	21.8±0.0	99.8	33.48	28,670	1.14E-12	0.61	7.706124 ±0.002573	1.459663 ±0.000547	0.019481 ±0.000109	0.022879 ±0.000502	0.000057 ±0.000008
1,150	21.8±0.0	99.52	40.7	300	1.09E-12	0.73	7.380466 ±0.002460	1.390698 ±0.000448	0.038294 ±0.000240	0.017928 ±0.000417	0.000125 ±0.000008
1,200	21.8±0.0	99.6	39.48	17,626	1.15E-12	0.85	7.830880 ±0.002016	1.476845 ±0.000521	0.019859 ±0.000072	0.019628 ±0.000717	0.000111 ±0.000008
1,250	21.9±0.0	99.32	33.78	11,129	7.03E-13	0.93	4.793186 ±0.001323	0.898329 ±0.000387	0.012216 ±0.000087	0.013953 ±0.000483	0.000115 ±0.000006
1,300	21.9±0.0	98.32	9.98	-44,945	2.41E-13	0.95	1.661811 ±0.000504	0.308251 ±0.000171	0.004054 ±0.000036	0.016204 ±0.000518	0.000099 ±0.000007
1,350	21.8±0.1	96.34	12.66	35,635	1.49E-13	0.97	1.046494 ±0.000519	0.191280 ±0.000152	0.002570 ±0.000067	0.007927 ±0.000437	0.000131 ±0.000007
1,425	21.8±0.0	97.87	21.4	-13,830	2.88E-13	1	1.990035 ±0.000583	0.368505 ±0.000193	0.004773 ±0.000039	0.009033 ±0.000586	0.000145 ±0.000007

Table 8. Tabulated radiometric data of RDD plagioclase

[Reduced with Taylor Creek Sanidine at 28.345 ± 0.012 Ma; Ma, mega-annum; $^{40}Ar^{*}$, radiogenic argon; ^{40}Ar—^{36}Ar, measured isotopes in volts (1.48E-13 moles/volt), corrected for blank, background, discrimination, and decay; temperature is in degrees Celsius]

Temp (°C)	Age(Ma)	%$^{40}Ar^{*}$	K/Ca	K/Cl	moles $^{40}Ar^{*}$	$\sum^{39}Ar$	^{40}Ar	^{39}Ar	^{38}Ar	^{37}Ar	^{36}Ar
600	18.2±1.1	23.19	0.14	63	6.77E-15	0.01	0.197260 ±0.000379	0.010472 ±0.000054	0.000946 ±0.000087	0.039302 ±0.001247	0.000523 ±0.000009
700	21.3±0.2	87.95	0.25	494	2.80E-14	0.03	0.215420 ±0.000188	0.036933 ±0.000081	0.000825 ±0.000044	0.076021 ±0.001288	0.000109 ±0.000007
800	21.3±0.1	95.45	0.25	1,424	5.96E-14	0.09	0.422769± 0.000220	0.078867 ±0.000091	0.001292 ±0.000046	0.162391 ±0.001055	0.000110 ±0.000007
900	21.4±0.1	96.47	0.28	1,520	1.08E-13	0.19	0.756103 ±0.000331	0.141596 ±0.000135	0.002287 ±0.000047	0.269735 ±0.002369	0.000164 ±0.000007
975	21.6±0.1	95.79	0.28	975	1.16E-13	0.29	0.816187 ±0.000343	0.150709 ±0.000127	0.002676 ±0.000058	0.284562 ±0.000966	0.000194 ±0.000007
1,050	21.6±0.0	98.67	0.29	975	1.70E-13	0.45	1.166163 ±0.000449	0.220845 ±0.000110	0.003898 ±0.000018	0.401824 ±0.003586	0.000163 ±0.000006
1,125	21.7±0.0	98.19	0.3	88	1.96E-13	0.63	1.347775 ±0.000508	0.253755 ±0.000125	0.015668 ±0.000066	0.447004 ±0.004308	0.000205 ±0.000007
1,200	21.7±0.0	97.86	0.3	147	1.84E-13	0.8	1.260850 ±0.000465	0.236243 ±0.000128	0.010032 ±0.000051	0.417970 ±0.002369	0.000206 ±0.000006
1,275	22.0±0.0	97.71	0.32	1,343	1.43E-13	0.92	0.989705 ±0.000318	0.182693 ±0.000134	0.003011 ±0.000020	0.296545 ±0.001579	0.000158 ±0.000007
1,350	22.3±0.1	94.59	0.28	3,305	8.57E-14	1	0.613041 ±0.000260	0.107991 ±0.000083	0.001588 ±0.000029	0.203359 ±0.000447	0.000168 ±0.000007

fig. 4). We prefer the recoil model age of 22.1 ± 0.2 m.y. as the best estimate for OTB eruption timing. This flow is interpreted to have erupted at or near the end of dome emplacement.

Sanidine from sample RWB yielded a climbing spectrum with a plateau at 21.7 ± 0.03 m.y. using 57.4 percent of the ^{39}Ar released. The isochron for these plateau steps is concordant at 21.7 ± 0.03 m.y. (tables 4, 5; fig. 5). We prefer the plateau date of 21.7 ± 0.03 m.y. for the eruption of this welded breccia RWB and its interpreted lateral equivalent, the ash-flow tuff of the Old State Road Member of the Fort Rock Creek Rhyodacite.

Plagioclase from sample RDD yielded a climbing age spectrum with ages ranging from 22.5 to21.3 Ma. Three concordant steps in the middle of the spectrum yield a plateau of 21.7 ± 0.03 m.y. using 50.1 percent of the ^{39}Ar released. The isochron for the three steps is concordant at 21.7 ± 0.1 m.y. (tables 4, 5; fig. 6). We prefer the plateau date of 21.7 ± 0.03 m.y. for the intrusion of this late-stage dike RDD in the Aquarius Mountains eruptive center.

Discussion

Volcanic rocks from the Fort Rock dome and Aquarius Mountains eruptive center are earliest Miocene. Ages are, from oldest to youngest, HTPA 22.3±0.03; OTB 22.1±0.2; RWB 21.7±0.03; and RDD 21.7±0.03 m.y. (table 4; figures 3–6). Radiometric ages for the HTPA, OTB, RWB, and RDD obey stratigraphic superposition within error, and were emplaced over a duration of ~0.6 million years. This relatively short duration is consistent with the absence of observed unconformities between HPTA and RWB, assuming that RWB is indeed the proximal equivalent of the Old Stage Member of the Fort Rock Creek Rhyodacite. Fuis (1996) documents fragments of felsic volcanic rocks within the upper part of the sedimentary breccia eroded from the uplifting Fort Rock dome ("sedimentary breccia of Noon Gorge"), suggesting that activity at the Aquarius Mountains eruptive center had begun before erosion of the dome had been completed. It is further documented that the ash-flow tuff of the Old Stage Road Member, the next major unit above the breccia shed from the dome, ponded around the Fort Rock dome at the same approximate elevation, suggesting that uplift of the dome was completed by the time of ash-flow eruption. The rhyodacite dike (RDD) represents the youngest felsic unit in and near the Aquarius Mountains eruptive center and cuts through both members of the Fort Rock Creek Rhyodacite. The similarity in age between RWB and RDD indicates that activity at the eruptive center was short-lived.

Ages from this study can be compared to other ages that have been obtained in the region of the Fort Rock dome and Aquarius Mountains. From west to east, these include the following:

1. An age of 18.78±0.02 m.y. for the Peach Spring Tuff (Ferguson and others, 2013). Description of this unit was first published by Young and Brennan (1974),

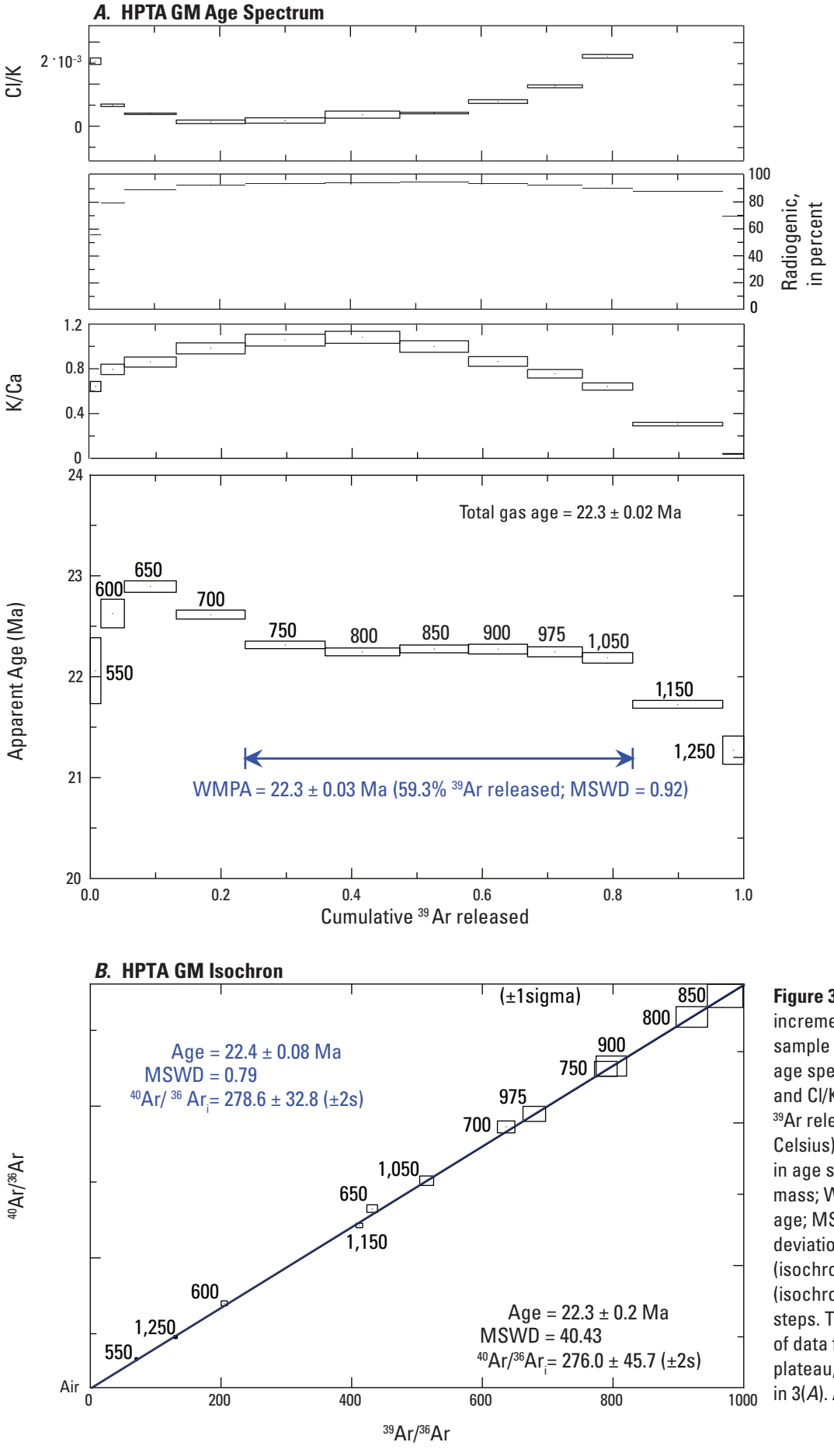

Figure 3. Graphs showing incremental heating results for sample HPTA. (*A*) Stacked $^{40}Ar/^{39}Ar$ age spectrum, K/Ca, radiogenic yield, and Cl/K plotted against cumulative ^{39}Ar released. Temperatures (degrees Celsius) labeled with each increment in age spectrum diagram. GM–ground mass; WMPA--weighted mean plateau age; MSWD–mean squared weighted deviation. (*B*) Isotope correlation (isochron) diagram. The black line (isochron) consists of data from all steps. The blue line (isochron) consists of data from only the steps on the plateau, indicated by the blue bracket in 3(*A*). Ar_i is the y intercept.

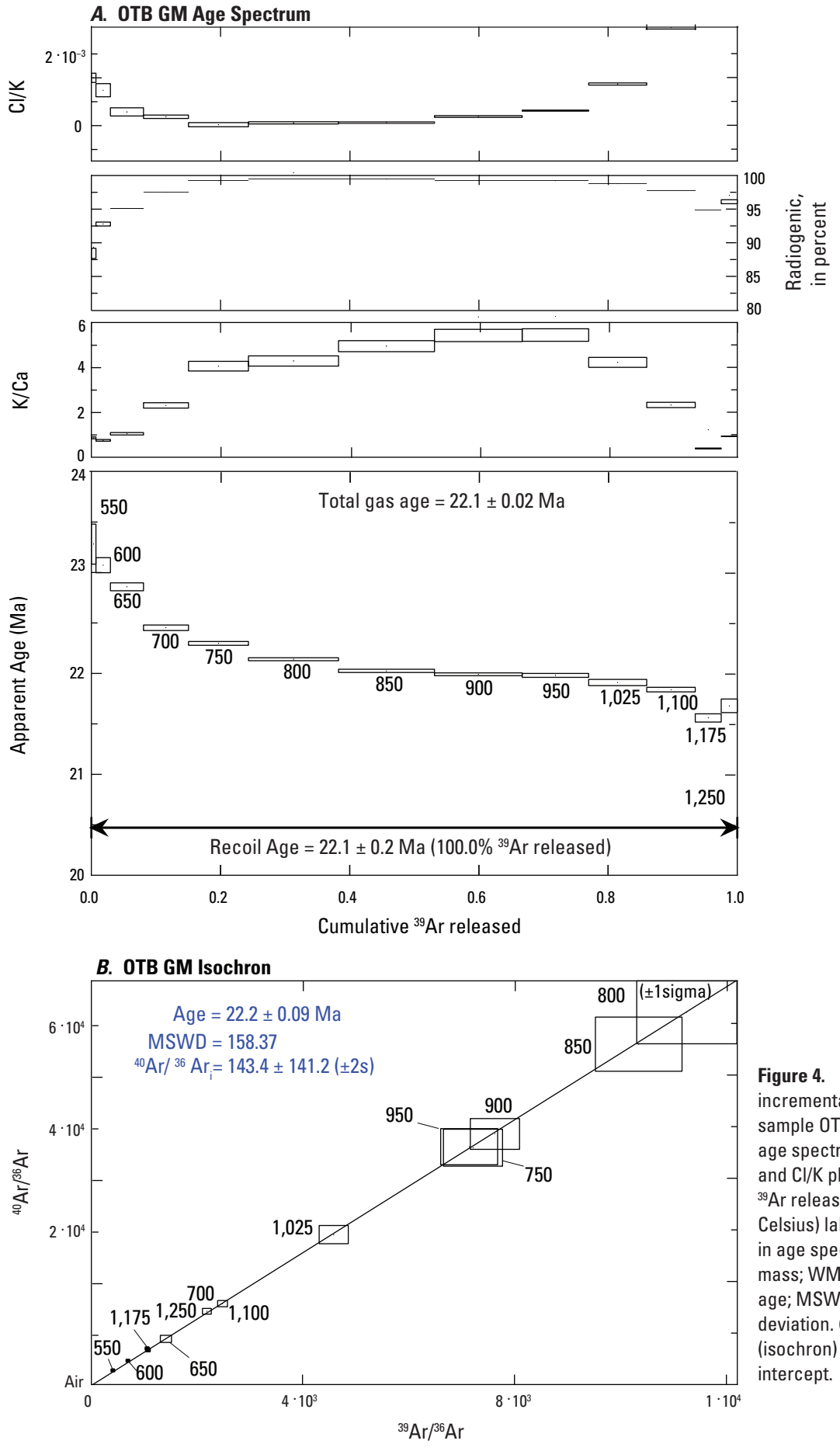

Figure 4. Graphs showing incremental heating results for sample OTB. (*A*) Stacked $^{40}Ar/^{39}Ar$ age spectrum, K/Ca, radiogenic yield, and Cl/K plotted against cumulative ^{39}Ar released. Temperatures (degrees Celsius) labeled with each increment in age spectrum diagram. GM–ground mass; WMPA--weighted mean plateau age; MSWD–mean squared weighted deviation. (*B*) Isotope correlation (isochron) diagram. Ar_i is the y intercept.

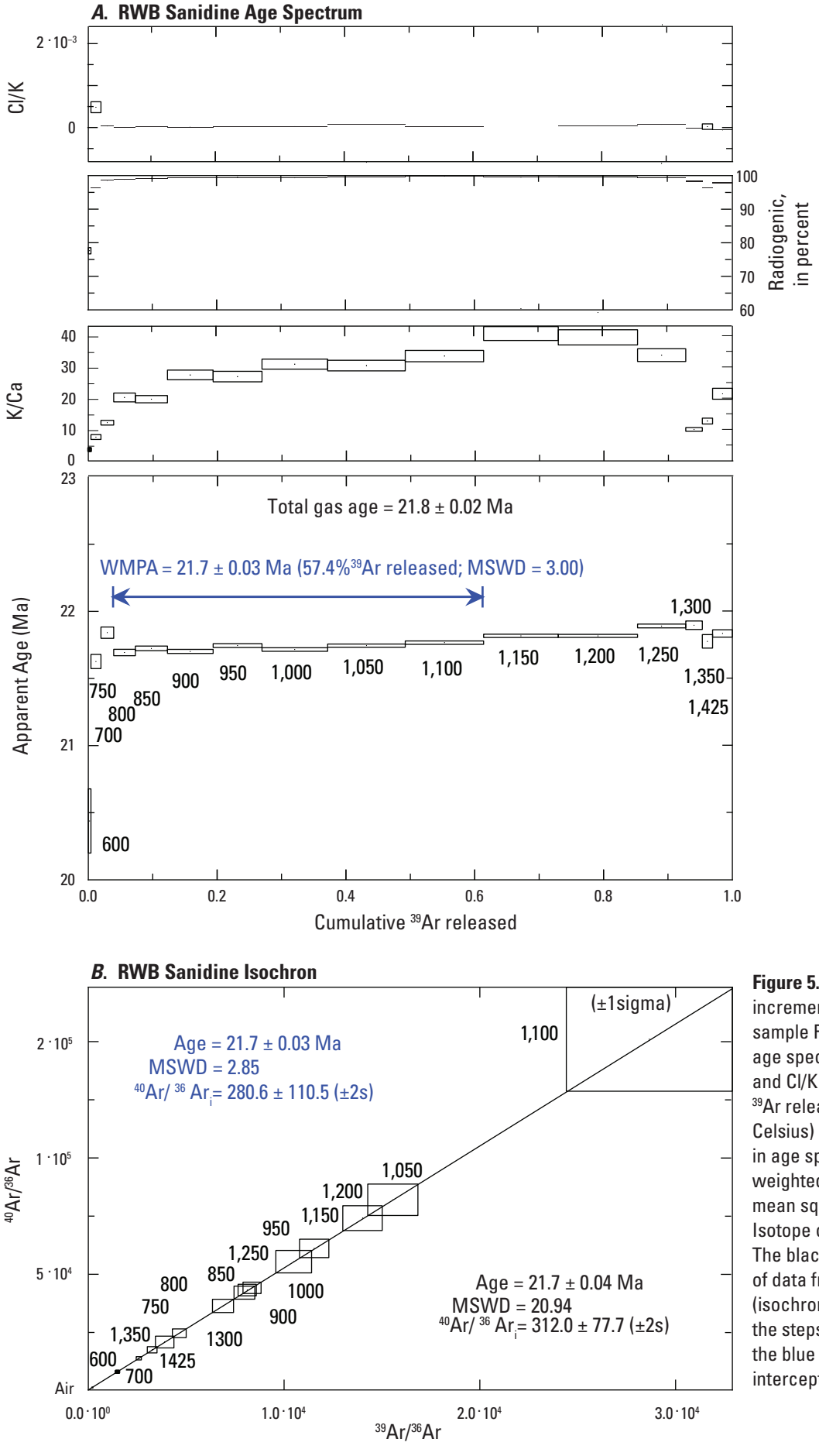

Figure 5. Graphs showing incremental heating results for sample RWB. (*A*) Stacked $^{40}Ar/^{39}Ar$ age spectrum, K/Ca, radiogenic yield, and Cl/K plotted against cumulative ^{39}Ar released. Temperatures (degrees Celsius) labeled with each increment in age spectrum diagram. WMPA–weighted mean plateau age; MSWD–mean squared weighted deviation. (*B*) Isotope correlation (isochron) diagram. The black line (isochron) consists of data from all steps. The blue line (isochron) consists of data from only the steps on the plateau, indicated by the blue bracket in 5(A). Ar_i is the y intercept.

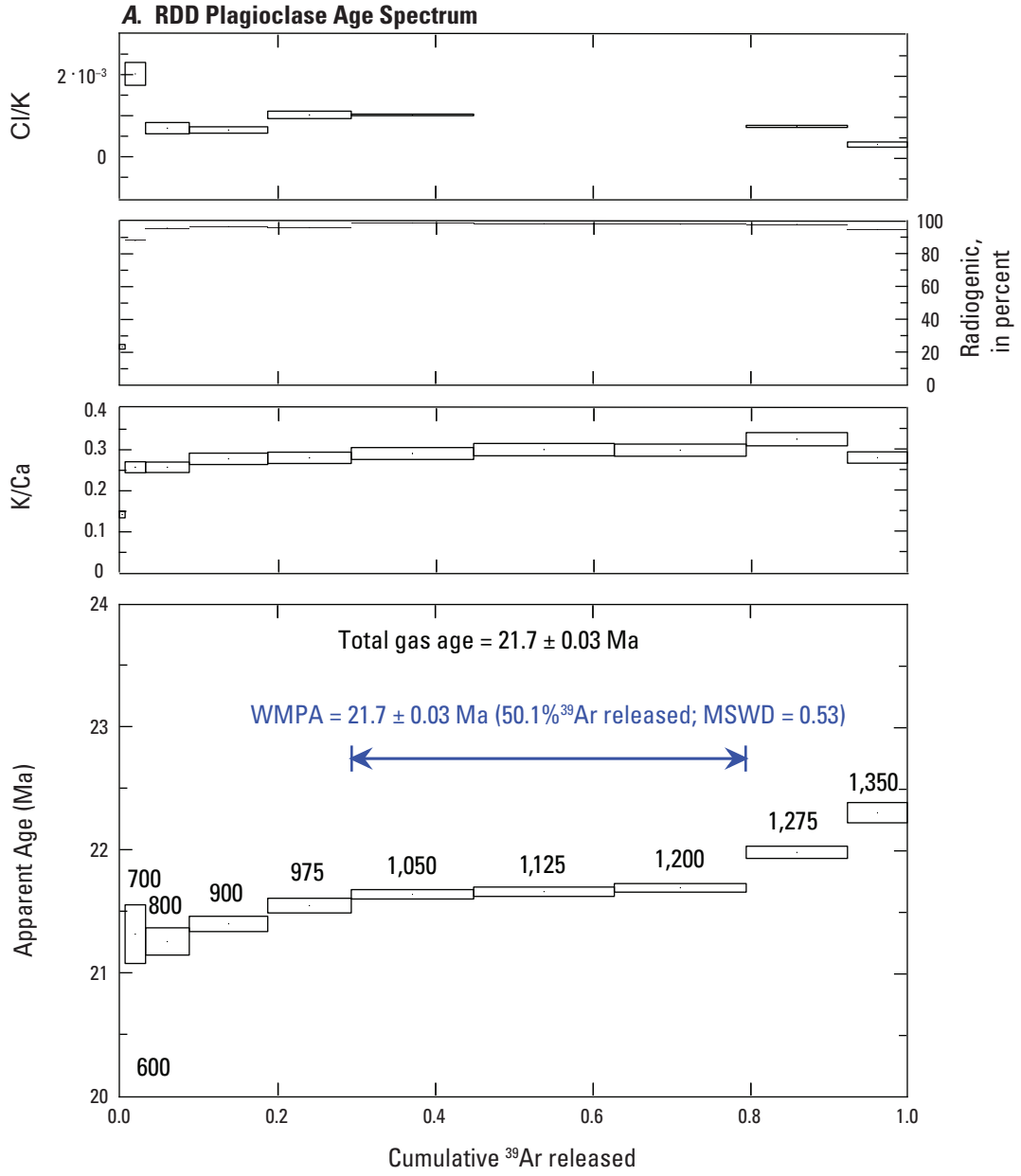

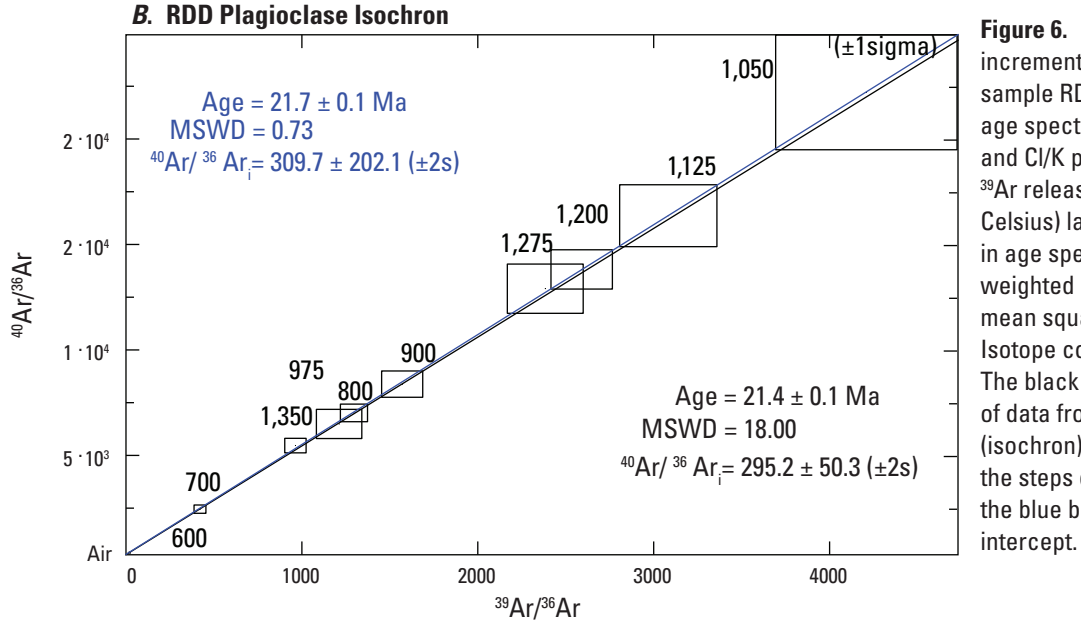

Figure 6. Graphs showing incremental heating results for sample RDD. (*A*) Stacked $^{40}Ar/^{39}Ar$ age spectrum, K/Ca, radiogenic yield, and Cl/K plotted against cumulative ^{39}Ar released. Temperatures (degrees Celsius) labeled with each increment in age spectrum diagram. WMPA–weighted mean plateau age; MSWD–mean squared weighted deviation. (*B*) Isotope correlation (isochron) diagram. The black line (isochron) consists of data from all steps. The blue line (isochron) consists of data from only the steps on the plateau, indicated by the blue bracket in 6(A). Ar_i is the y intercept.

with a K-Ar age of 17.6 Ma. Outcrops in the Aquarius Mountains are as much as 100 km east of the caldera source, that is located in the Black Mountains, 40 km WSW of Kingman, Ariz. At Penitentiary Butte, located 16 km west of the center of the Fort Rock dome, the Peach Spring Tuff forms a cap rock. It rests above an unconformity atop the Three Sisters Butte Member of the Fort Rock Creek Rhyodacite (Fuis, 1996). This unconformity would represent approximately 2.9 Ma. Five km farther west of Penitentiary Butte, across a major north-south Basin and Range fault that extends southward from the foot of the Cottonwood Cliffs, the Peach Spring Tuff rests on both mafic igneous rocks similar to the Crater Pasture Formation and on Precambrian igneous and metamorphic rocks, at an elevation well below its outcrop on Penitentiary Butte (Fuis, 1996). It is interpreted that the block west of the Basin and Range fault first moved upward after deposition of the Fort Rock Creek Rhyodacite, allowing removal of this unit, followed by emplacement of the Peach Spring Tuff. Finally, the block west of this fault moved downward to produce the relationships seen today (Fuis, 1996).

2. An age of 22.0 ±0.7 m.y. for a hornblende-olivine basalt dike that intrudes part of the Fort Rock Creek Rhyodacite 12 km northwest of the center of the Fort Rock dome (sample F78-85; Goff and others, 1983; our table 1). This date is consistent with the geologic relationships seen at this location, namely, the dike is younger than both the Fort Rock Rhyodacite and Crater Pasture Formation, given the error bar on its age.

3. An age of 20.7±0.6 m.y. for a basaltic andesite flow(?) approximately 11 km NNW of the center of the Fort Rock dome (sample BA78-73; Goff and others, 1983; our table 1). This unit is interpreted by Goff and others (1983) to be equivalent to basalts overlying (and possibly interfingering with) the Peach Spring Tuff as exposed farther north.

4. An age of 22.4±0.8 m.y. for a biotite-pyroxene andesite intrusive (vent) rock approximately 8 km north of the center of the Fort Rock dome (sample F78-88; Goff and others, 1983; our table 1). This unit is overlain and surrounded by younger basalt flows. Given its age, this unit appears laterally equivalent to the Crater Pasture Formation.

The last 3 ages are potassium-argon ages obtained by Daniel Krummenacher, San Diego State University, Calif. (Goff and others, 1983).

Rocks in the Mohon Mountains and Hope Mountain volcanic fields south and southeast of Fort Rock dome (fig. 1) range in age from 22-5 m.y. (Simmons, 1990; Simmons and Ward, 1992). Rocks dated between 22 and 20 m.y. consist primarily of trachyandesite and dacite breccias and form the two large stratovolcanoes in the Mohon Mountains volcanic field. Volcanic rocks younger than 13 m.y. comprise a bimodal suite of alkalic basalt and high-silica rhyolite and form two large volcanic domes in these fields. The bulk of the volcanic rocks of these fields overlie the Peach Spring Tuff, which is exposed in the walls of Trout Creek (fig. 1).

Summary

New radiometric ages of samples taken from the Fort Rock dome and Aquarius Mountains eruptive center fall within a short time span of 0.6 m.y. in the earliest Miocene. Fort Rock dome emplacement followed eruption of seven intermediate to ultramafic lava flows by as little as 0.2 m.y. During the waning period of dome uplift and erosion, felsic eruptive activity began at the nearby Aquarius Mountains rhyodacite eruptive center. Most eruptive activity at the Aquarius Mountains eruptive center occurred in a short time interval (0.03 m.y.) around 21.7 Ma. The ages reported here all predate the Peach Spring Tuff (18.78 Ma), which overlies the Fort Rock Creek Rhyodacite in this region. The Peach Spring Tuff in turn underlies the bulk of the Mohon Mountains volcanic field south of the Fort Rock dome and Aquarius Mountains.

Acknowledgments

Reviews by Seth Burgess, John Tinsley, and Keith Knudsen improved this manuscript significantly and were much appreciated. Editing and formatting by Phil Frederick and Kimber Petersen were very helpful and got this manuscript to its final form. Luke Blair kindly drafted the index map (fig. 1).

References Cited

Dalrymple, G.B., 1989, The GLM continuous laser system for $^{40}Ar/^{39}Ar$ dating; description and performance characteristics, *in* Shanks, W.C., III, and Criss, R.E., eds., New frontiers in stable isotopic research; laser probes, ion probes, and small-sample analysis: U.S. Geological Survey Bulletin 1890, p. 89–96.

Dalrymple, G.B. and Duffield, W.A., 1988, High precision $^{40}Ar/^{39}Ar$ dating of Oligocene rhyolites from the Mogollon-Datil volcanic field using a continuous laser system: Geophysical Research Letters, v. 15, p. 463–366.

Dalrymple, G.B., Alexander E.C., Jr., Lanphere, M.A., and Kraker, G.P., 1981, Irradiation of samples for $^{40}Ar/^{39}Ar$ dating using the Geological Survey TRIGA reactor: U.S. Geological Survey, Professional Paper 1176. 55 p.

Ferguson, C.A., McIntosh, W.C., and Miller, C.F., 2013, Silver Creek caldera—The tectonically dismembered source of the Peach Spring Tuff: Geology, v. 41, p. 3–6.

Fleck, R.J., Hagstrum, J.T., Calvert, A.T., Evarts, R.C., and Conrey, R.M., 2014, $^{40}Ar/^{39}Ar$ geochronology, paleomagnetism, and evolution of the Boring volcanic field, Oregon and Washington, USA: Geosphere, v. 10, no. 6, p. 1283–1314.

Fleck, R.J. and Calvert, A.T., 2016, Intercalibration of $^{40}Ar/^{39}Ar$ mineral standards with Bodie Hills Sanidine: Geological Society of America Abstracts with Programs. v. 48, no. 7, Paper no. 238-4, https://doi.org/10.1130/abs/2016AM-286011.

Fuis, G. S., l973, The geology and mechanics of formation of the Fort Rock dome, Yavapai County, Arizona: Pasadena, California Institute of Technology, Ph.D. dissertation, 278 p.

Fuis, G. S., 1996, The geology and mechanics of formation of the Fort Rock Dome, Yavapai County, Arizona: U.S. Geological Survey Professional Paper 1266, 95 p., 2 pl., scale 1:5000.

Goff, F.E., Eddy, A.C., and Arney, B.H., 1983, Reconnaissance geologic strip map from Kingman to south of Bill Williams Mountain, Arizona: University of California, Los Alamos National Laboratory, LA-9202-MAP, 6 sheets, scale 1:48,000.

Renne, P.R., Swisher, III, C.C., Deino, A.L., Karner, D.B., Owens, T., and DePaolo, D.J., 1998, Intercalibration of standards, absolute ages, and uncertainties in $^{40}Ar/^{39}Ar$ dating: Chemical Geology, v. 145, p. 117–152.

Sauck, W.A., and Sumner, J.S., 1971, Residual aeromagnetic map of Arizona: Tucson, University of Arizona, Department of Geosciences, scale 1:1,000,000.

Simmons, A.M., 1990, The Miocene Mohon Mountains volcanic field, west-central Arizona—geology, geochemistry, and petrogenesis: State University of New York at Buffalo, Ph.D. dissertation, 294 p.

Simmons, A.M., and Ward, A.W., 1992, Preliminary geologic map of the Mohon Mountains volcanic field, Mohave and Yavapai Counties, Arizona: U.S. Geological Survey Open-File Report 92–198, 2 plates, scale 1:50,000.

Young, R.A., and Brennan, W.J., 1974, Peach Springs Tuff—Its bearing on structural evolution of the Colorado Plateau and development of Cenozoic drainage in Mohave County, Arizona: Geological Society of America Bulletin, v. 85, p. 83–90.

Young, R.A., and McKee, E.H., 1978, Early and middle Cenozoic drainage and erosion in west-central Arizona: Geological Society America Bulletin, v. 89, p. 1745–1750.

Menlo Park Publishing Service Center, California
Manuscript approved for publication April 15, 2019
Edited by Phil Frederick
Layout and design by Kimber Petersen

ISSN 2331-1258 (online)
https://doi.org/10.3133/ofr20191038